Environmental Science
Water Research & Technology

Low concentrations of Cu2+ in synthetic nutrient containing wastewater inhibit MgCO3-to-struvite transformation

Journal:	*Environmental Science: Water Research & Technology*
Manuscript ID	EW-ART-11-2020-001035.R1
Article Type:	Paper

Recovering nutrients from wastewater is an emerging field of interest due to the impact modern agriculture has on aquatic ecosystems. This work presents the impact of transition metals (Cu and Zn which are common contaminants in municipal and industrial wastewater) being present at the heterogeneous interface of struvite crystallization ($MgNH_4PO_4.6H_2O$) on magnesite ($MgCO_3$).

Low concentrations of Cu^{2+} in synthetic nutrient containing wastewater inhibit $MgCO_3$-to-struvite transformation

Karolina Barčauskaitė,[1,2] Donata Drapanauskaitė,[1,2] Manoj Silva,[1] Vadim Murzin,[3,4] Modupe Doyeni,[2] Marius Urbonavicius,[5] Clinton F. Williams,[6] Skaidrė Supronienė[2] and Jonas Baltrusaitis[1,*]

[1]Department of Chemical and Biomolecular Engineering, Lehigh University, B336 Iacocca Hall, 111 Research Drive, Bethlehem, PA 18015, USA
[2]Lithuanian Research Centre for Agriculture and Forestry, Instituto al.1, LT-58344, Akademija, Kedainiai District, Lithuania
[3]Bergische Universität Wuppertal, Gaußstraße 20, D-42119, Wuppertal, Germany
[4]Deutsches Elektronen Synchrotron DESY, Notkestraße 85, D-22607 Hamburg, Germany
[5]Center for Hydrogen Energy Technologies, Lithuanian Energy Institute, 3 Breslaujos, 44403 Kaunas, Lithuania
[6]USDA-ARS, US Arid Land Agricultural Research Center, 21881 N. Cardon Ln, Maricopa, AZ, 85138, USA

Abstract
Simultaneous major nutrient nitrogen (N) and phosphorous (P) recovery from wastewater is key in achieving food-energy-water sustainable development. In this work, we elucidate the reaction kinetics, crystalline structure and chemical composition of the resulting solid precipitate obtained from simulated N and P containing wastewater solution using widely abundant low solubility magnesite ($MgCO_3$) particles in the presence of the common transition metal ions, such as zinc (Zn^{2+}) or copper (Cu^{2+}). We show that up to 100 ppm Zn^{2+} from the simulated wastewater can be incorporated into the struvite lattice as isolated distorted Zn^{2+} while even at very low concentrations of ~5 ppm Cu^{2+} ions almost completely inhibit struvite crystal formation. The resulting solid precipitate distinctly affects soil microbial biomass carbon and soil dehydrogenase enzyme activity. These results show a cautionary case where abundant natural mineral $MgCO_3$ exhibits very different chemistry in Cu^{2+} containing simulated wastewater and does not readily adsorb or retain NH_4^+ and PO_4^{3-} ions, unlike less sustainable but more water-soluble magnesium source, such as $MgCl_2$, at the equivalent molar $[Mg^{2+}]:[NH_4^+]:[PO_4^{3-}]$ ratio of [1.4:1:1].

*Corresponding author: job314@lehigh.edu, phone +1-610-758-6836

Keywords: $MgCO_3$; struvite; wastewater; Cu; Zn; dehydrogenase activity

Introduction. Modern agricultural practices and increasing use of mineral fertilizers have significantly perturbed the global nitrogen (N) and phosphorus (P) cycles.(1) Due to soil bacteria activity, a loss of up to 90% of the applied N can take place.(1–3) Concomitantly, ammonia synthesis using air N_2 requires 4% of the world's annual natural gas supply as well as 1% of the annual global energy production.(4) P, on the other hand, is mined from rock and it is dwindling without replenishment.(5,6) P fertilizers are much less water-soluble and enter the watershed via runoff.(7) Therefore, producing green fertilizer materials more stable in the environment becomes important in promoting sustainable agricultural practices.(8–11) Specifically, producing fertilizer containing both N and P from wastewater streams is an important aspect of sustainable development.

Struvite ($MgNH_4PO_4{\cdot}6H_2O$) synthesis is a unique opportunity that allows for the simultaneous removal of both N-NH_4^+ and P-PO_4^{3-} from wastewater streams. It is a low solubility fertilizer that is a more environmentally-sustainable, compared to the conventional N fertilizers which have the propensity to volatilize and emit greenhouse gases.(12–15) Struvite precipitation from the wastewater so far chiefly utilized soluble magnesium precursors, such as magnesium chloride ($MgCl_2$), which also require wastewater pH adjustment with external chemicals, such as NaOH. Earth-abundant low solubility magnesium sources, such as periclase (MgO),(10,16–18) magnesite ($MgCO_3$),(19,20) brucite ($Mg(OH)_2$),(21) and dolomite ($CaMg(CO_3)_2$)(13,22,23) have also been reported to form struvite from model wastewater containing NH_4^+ and PO_4^{3-} albeit under distinctly different reaction kinetics. Due to their alkaline nature, upon partial dissolution, they result in the solution pH increase and do not require added NaOH. However, anthropogenic wastewater has a complex chemical composition and contains transition metal ions originating from industrial, municipal and agricultural activities.(24) Copper (Cu) and zinc (Zn) are of particular interest given their presence in sewage sludge from domestic and industrial wastewaters, which is often a feedstock of interest for nutrient capture since it is rich in N and P.(25) Studies have reported Cu^{2+} and Zn^{2+} concentration in municipal wastewater from 10-90 ppb to 49-498 ppb respectively.(26) However, sewage sludge obtained from mixed domestic and industrial wastewater averaged 1700 ppm of Zn and 500 ppm of Cu^{2+},(27) while the sewage sludge of a municipal stormwater treatment plant contained up to 500 ppm of Zn^{2+} and 50 ppm of Cu^{2+}.(28) These relatively low concentrations of Cu^{2+} and Zn^{2+} were shown to not result in significant struvite morphological changes when using $MgCl_2$, despite the kinetic hindering effects.(29) Structurally, Zn^{2+} can be

incorporated into the solid precipitate crystal lattice or sorbed on the surface during struvite precipitation from separated sewage sludge anaerobic digester effluent using $MgCl_2$ reducing the purity of the solid precipitate.(30–34) Previous studies on struvite synthesis using $MgCl_2$ in the presence of Zn^{2+} and Cu^{2+} aqueous ions have also shown that these metals are incorporated into the struvite as phosphate and hydroxide phases.(32–34) For example, Peng *et. al.* demonstrated that in the presence of Cu^{2+} concentrations from 200 ppm to 800 ppm $Cu(OH)_2$ was formed in addition to struvite.(35) Rouff *et al.* investigated the structure of these metals in synthesized struvite using $MgCl_2$ and found polymeric Zn-units even at low concentrations.(32) Further studies by the same authors showed that Cu^{2+} also is incorporated into the struvite structure, but was affected by the organic matter content in the wastewater.(33) Notably, water-soluble $MgCl_2$ was predominantly used and the effects of Zn^{2+} and Cu^{2+} on struvite formation kinetics and the resulting crystal structure using low solubility Mg minerals were largely not studied. While some reports have claimed that struvite formed from wastewater does not contain significant heavy metal concentrations,(36) it is now evident that the concentration of metals in the wastewater plays an important role and can result in significant adsorption into the solid struvite(33,34) which can have detrimental effects on soil biota.

The accumulation and bioavailability of heavy metals in the food chain depend on various environmental factors such as temperature and physicochemical properties of the soil such as organic matter content, pH, cationic exchange capacity.(37) This work aims to investigate the effects of Cu^{2+} and Zn^{2+} on struvite formation kinetics from simulated wastewater and product distribution using low solubility magnesium-containing minerals, such as $MgCO_3$, rather than water-soluble salts, such as $MgCl_2$, as well as on such struvite effects on soil biome. In particular, studies were performed to assess the impact of Cu^{2+} and Zn^{2+} incorporated struvite synthesized using $MgCO_3$ on dehydrogenase activity (DHA) and soil microbial biomass carbon (SMBC) in soil. The unexpected soil biota testing results were further elucidated by interrogating the struvite formation reaction kinetics using ion chromatography to assess NH_4^+ and PO_4^{3-} ion removal from simulated wastewater solution while the resulting Cu^{2+} and Zn^{2+} concentration in the solid precipitate were measured using inductively coupled plasma mass spectroscopy (ICP-MS). The resulting struvite crystalline structure was analyzed using powder X-ray diffraction (XRD), the particle morphology and elemental analysis using electron microscopy (SEM/EDS) while the

atomic information on the structure of the metals was probed using X-ray absorption spectroscopy (XAS).

Experimental Methods

Reagents and solutions. Magnesium carbonate ($MgCO_3$) (magnesite), magnesium as MgO ≥ 40 % and monoammonium phosphate ($NH_4H_2PO_3$) ≥ 98 % were purchased from Sigma-Aldrich. Copper (II) nitrate trihydrate ($Cu(NO_3)_2 \cdot 3H_2O$) ≥ 99.5 % and nitric acid (HNO_3) 65 % were obtained from Merck. Zinc nitrate hexahydrate ($Zn(NO_3)_2 \cdot 6H_2O$) 98 % was obtained from Acros Organics.

Struvite synthesis. The synthesis procedure is shown in **Figure 1**. In particular, struvite synthesis from simulated wastewater was performed using low solubility abundant magnesite mineral. Cu- and Zn-containing struvites were synthesized using copper (II) nitrate trihydrate and zinc (II) nitrate hexahydrate. Stock solution containing 1000±1 ppm of monoammonium phosphate ($NH_4H_2PO_4$) was used. The weighed solid Cu^{2+} or Zn^{2+} amounts were added into the prepared 1000 ppm MAP solution to result in the final concentration of 2±0.02, 5±0.05, 10±0.1 or 20±0.2 ppm for Cu^{2+} and 100±0.5 ppm for Zn^{2+} with constant stirring at 400 rpm. 1000 ppm MAP represents PO_4^{3-} and NH_4^+ values found in municipal, animal and industrial wastewater(38) while maintaining above the molar 1:1 ratio needed for struvite formation. Finally, $MgCO_3$ powder was added at 1000 ppm concentration to the simulated wastewater and stirred for up to 120 minutes. The total volume of the reactive solution was 750 mL. 1.5 mL of solution was sampled periodically and filtered through a 25 mm nylon filter (0.45 µm size) to remove solid precipitate. The filtrate was diluted 5 times with 2 % HNO_3 and analyzed by ICP-MS for Zn and Cu content and residual Mg^{2+}, PO_4^{3-} and NH_4^+ ions using IC.

Ion chromatography. The Shimadzu HIC-20A Super ion chromatography system (Kyoto, Japan) was used in all experiments to measure Mg^{2+}, NH_4^+ and PO_4^{3-} ions. Separation columns used were Shim-pack IC-SC1 (4.6×150mm) with Guard column Shim-pack IC-SC1 (G) (4.6×10mm) for cation analysis and Shim-pack IC-SA2 (4.0×250mm) with Guard column Shim-pack SA2 (G) (4.6×10mm) for anion analysis. The sample-loop volume was 1000 uL in cation and anion systems and eluted species were measured using electric conductivity detector CDD-10ASP. 1.8 nM Na_2CO_3/1.7 mM $NaHCO_3$ was used as eluent for anion analysis while 0.7 mM methanesulfonic acid for cation analysis. All samples were measured at room temperature. The system was

computer-controlled through LabSolution software. Error bars represent uncertainty from three independent measurements.

Inductively coupled plasma mass spectrometer (ICP-MS) analysis. Solid precipitate samples were digested using microwave-assisted extraction (MAE) by means CEM MARS 6® (Matthews, NC, USA) digestion system equipped with a 100 mL Teflon vessel. Approximately, 0.1 g of solid struvite sample was accurately weighed into a Teflon vessel and digested using 10 mL of analytical grade concentrated nitric acid (≥ 65%) (Sigma-Aldrich, Germany). Before digestion, the samples were soaked in acid for 30 min at room temperature. Digestion was performed under the following conditions: temperature – 200°C; pressure – 800 psi; ramp time – 15 min; hold time – 20 min; microwave power – 1600W. The digested samples were cooled down and thoroughly transferred into 100 mL volumetric flask and diluted using bidistilled water till the mark. The blank sample was included in each digestion run. To measure concentrations of Mg, P, Cu and Zn inductively coupled plasma mass spectrometer (ICP-MS) was operated at standard mode. Samples were introduced from an autosampler incorporating an ASXpress™ rapid uptake module (Cetac ASX-520, Teledyne Technologies Inc., USA) through a PEEK nebulizer (Burgener Mira Mist, Mississauga, Burgener Research Inc., Canada). Analyzed elements were estimated using an external multi-element six-point calibration curve in the range 50–2000 ppb (50, 100, 200, 500, 1000, 2000 ppb). The standard mixture solution of multiple microelements (Mg, P, Cu, Zn) in 2 % nitric acid was obtained from CPAchem (Bulgaria). Double distilled water was obtained using the distillation apparatus Thermo Scientific (USA) and used for dilution in all cases.

Powder X-ray diffraction. The crystal structure of samples was analyzed via X-ray diffraction (XRD) method using a Bruker D8 diffractometer (40 kV, 40 mA) operated in the θ–θ configuration. The measurements were performed at 2θ angle in the scan range of 20 – 70° using Cu cathode Kα radiation (λ = 0.15406 nm) in steps of 0.01° and Lynx eye position-sensitive detector.

Scanning electron microscopy. The morphology of the struvite surface was examined with a scanning electron microscopy (SEM, Hitachi S-3400N) using a secondary electron detector at an accelerating voltage of 3 kV. Energy-dispersive X-ray spectroscopy (EDS, Bruker Quad 5040) was used for the analysis of the elemental mapping of samples.

X-ray Absorption Near Edge Spectroscopy (XANES) and Extended X-ray Absorption Fine Structure (EXAFS) measurements were performed at the Advanced X-ray Absorption

Spectroscopy Beamline P64 (PETRA III ring, DESY, Hamburg).(39) Samples were mixed with microcrystalline cellulose and pressed into powder pellets. Spectra were measured at room temperature in continuous acquisition mode when the undulator and the monochromator movements were synchronized on the fly. Three ionization chambers were filled with pure nitrogen to reduce sensitivity to higher harmonics of the undulator. For each set of samples, the corresponding metal foil (Cu or Zn) was used as a standard between the second and the third ionization chambers. The monochromatic beam flux on the sample was ca. $5x10^{12}$ photons/s. The time for each spectrum was set to 5 minutes; an average of 3-4 scans was used for the analysis.

Experimental EXAFS spectra were fitted using IFEFFIT and LARCH packages.(40,41) In the fitting procedure *ab initio* photoelectron backscattering amplitudes and phases were calculated self-consistently using FEFF8.5 code.(42) EXAFS functions were k^2 and k^3 – weighted and fitted in 1.0-3.0 Å interval of R-space. The range of photoelectron wave vectors used in the fit was 3.0–15.0 $Å^{-1}$. The amplitude reduction factor S_0^2 was obtained from the fit of the first shell of the corresponding standard (0.87 for Cu, 0.85 for Zn). Coordination numbers were fixed, different models with different coordination numbers were tested, the best model and fit were taken. Debye-Waller factors, σ^2, distances, R, and the total energy shift, ΔE_0, were varied during the fit.

Soil microbial biomass activity measurements. The soil was collected from the experimental field site at the Institute of Agriculture, Lithuania Research Centre for Agriculture and Forestry (55°40′ N, 23°87′ E). The soil was Endocalcari-Epihypogleyic Cambisol characterized by a homogeneous texture. Soil samples (0-20 cm) were collected and visible plant debris, soil animals and stones were manually removed from the field moist soil samples. The remaining soil was thoroughly mixed, air-dried at room temperature, passed through a 2-mm sieve and adjusted to 40% water holding capacity (WHC) by adding deionized water.

The soil was introduced into polyvinyl chloride trapezoidal-section containers (chemically inert and opaque to light), of approximately 1 L capacity and the soil layer was separated from the container using a paper mesh. To evaluate struvite effect on soil microorganism activity and microbial biomass content, pots with soil and struvite synthesized using various precursors were stored under controlled climate conditions in laboratory incubators (CLIMACELL 707, MMM Medcenter Einrichtungen GmbH, Munich, Germany). Laboratory incubator parameters were set for a day and night mode as follows: temperature 23±0.5 º C during the day and 18±0.5 ºC during

the night, RH 68±2 %, fan mode on 100 %, light on during the day and light off during the night. Deionized water was regularly added to the pots to maintain the water content at 40% WHC. Soil samples for soil dehydrogenase enzyme activity and soil microbial biomass carbon determination were taken after 0, 5, 28 and 48 days. The measured organic carbon content was 1.30±0.15 %, total N 0.14±0.02 %, P_2O_5 and K_2O concentrations were 134.00±6.56 mg kg^{-1} and 142.67 mg kg^{-1}, respectively. The measured pH was 7.03±0.15. The soil contained 4139±955 mg kg^{-1} of Ca and 947±258 mg kg^{-1} of Mg. Approximately 1000 g of soil was mixed with struvite and struvite synthesized using Cu^{2+} and Zn^{2+} precursors. The amount of struvite was calculated according to nitrate directive 91/676/EEC to obtain 170 kg of N per one hectare. The pot experiments were in triplicates with four amendments namely, control (soil without struvite), soil + struvite, soil + struvite which contains Zn^{2+} ions and soil + struvite which contains Cu^{2+} ions. The overview of testing procedures is shown in **Figure 2.**

Soil dehydrogenase enzyme activity (DHA) measurements. Dehydrogenase activity was determined according to the slightly modified method described earlier.(43) The collected soil samples were air-dried, homogenized and analyzed the same day. 20 g of air-dried soil and 0.2 g of $CaCO_3$ were thoroughly mixed. 6 g each of this mixture was dispensed into the three test tubes (three replicates of each sample). To each tube, 1 ml of 3 % 2,3,5-triphenyl tetrazolium chloride (TTC) aqueous solution and 2.5 ml distilled water were added. The contents of each tube were mixed with a glass rod then the tube was stoppered and incubated at 37 ºC for 24 hours. After 24 hr, the stopper was removed, 10 ml methanol was added and the tube was shaken for 1 min using vortex (IKA, Germany). The filtrate was transferred into a glass funnel and filtered to a 50 ml volumetric flask. The filtrate was diluted through the funnel to a 50 ml volume into the volumetric flask using methanol. The intensity of the red color was measured using a UV-Vis spectrophotometer (Shimadzu, Japan) using a wavelength of 485 nm in a 1 cm cuvette with methanol as a blank reference. The amount of triphenyl formazan (TPF) produced by soil samples was estimated using the calibration curve prepared using 5 to 50 µg ml^{-1} of TPF.

Soil microbial biomass carbon (SMBC) determination using fumigation extraction method. SMBC was determined using the fumigation-extraction method.(44),(45) 20 g of soil was fumigated via exposing the soil to the alcohol-free $CHCl_3$ vapor in a sealed vacuum desiccator for 24 hr. The fumigated soil was evacuated repeatedly in a clean empty desiccator until the odor of

$CHCl_3$ was no more detected and then extracted with 80 ml of 0.5M K_2SO_4 (soil:K_2SO_4 = 1:4) for 30 min by oscillating shaking at 200 rpm and then filtered through a Whatman No. 42 filter paper. Organic carbon content in the extracts was measured using the dichromate digestion method. 2 ml of $K_2Cr_2O_7$ (66.7mM) and 15 ml of the digestion mixture (2:1 conc. H_2SO_4:H_3PO_4 (v/v)) was added to 8 ml of extract in a 250 ml conical flask. The mixture was gently refluxed for 30 min, allowed to cool and diluted with 20 ml distilled water. The excess $K_2Cr_2O_7$ was measured by titration with ferrous ammonium sulfate (40.0mM) using a 1.10-phenanthroline-ferrous sulfate complex (25mM) solution as an indicator. The extraction of non-fumigated soil was the same as that of the fumigated soil. SMBC was calculated from the differences in extractable organic carbon (OC) between the fumigated and non-fumigated soil sample with a conversion factor (KEC) of 0.38.(44) SMBC was calculated as

$$SMBC = Ec/KEC \quad (1),$$

where Ec = (OC extracted from fumigated soil) - (OC extracted from non-fumigated soil) and KEC = 0.38(44) (2).

Statistical analysis. Pairwise differences, analysis of variance (ANOVA) with Turkey's studentized range tests were calculated using the SAS program suite (SAS Institute Inc., USA). Pearson's correlation coefficients were used to investigate relationships between selected variables. Mean ± SE (standard error of the mean) was used to describe the variability of measurements.

Results and Discussion

Struvite synthesis and characterization.

Kinetics of PO_4^{3-} and NH_4^+ adsorption on $MgCO_3$ in the presence of Cu^{2+} and Zn^{2+}. Struvite synthesis was performed using 1000 ppm $MgCO_3$ and 1000 ppm MAP with and without 5 and 20 ppm Cu^{2+} and 100 ppm Zn^{2+} at otherwise identical conditions with no external pH adjustment. The concentrations of both metals were chosen to represent nutrient-containing wastewater to represent moderately contaminated sewage sludge.(27,28) The synthesized materials were dried under room temperature. The solid precipitate formed was analyzed for the crystalline structure, heavy metal content and local atomic coordination structure.

First, ion chromatography was used to monitor the time-dependent anion (PO_4^{3-}) and cation (NH_4^+ and Mg^{2+}) concentration change taking place in the liquid phase during the formation of solid precipitate. **Figure 3a** shows the concentration profile of residual PO_4^{3-} ions with initial $MgCO_3$ concentration of 1000 ppm and 1000 ppm $NH_4H_2PO_4$ corresponding to molar $[Mg^{2+}]:[NH_4^+]:[PO_4^{3-}]$ ratio of [1.4:1:1]. This was chosen after testing a wide range of the initial $MgCO_3$ concentrations to efficiently supersaturate the solution to form struvite.(19) The concentration profile of PO_4^{3-} showed a steep decrease in the presence of $MgCO_3$ alone and the presence of 100 ppm Zn^{2+}. Notably, reaction kinetics was completely inhibited for 100 ppm Zn^{2+} case for at least 25 min after the reaction started, as evidence via plateau in the curve. Somewhat unexpectedly, virtually no change in the initial PO_4^{3-} concentration was observed when 20 or 5 ppm Cu^{2+} was present. Only notable decrease to ~600 ppm PO_4^{3-} was measured after 100 min in the presence of 5 ppm Cu^{2+} suggesting very slow reaction kinetics. $MgCO_3$ alone exhibited the fastest rate of PO_4^{3-} removal from solution, with the PO_4^{3-} concentration of 150 ppm at the equilibrium, after 2 hours. The time-resolved plot of NH_4^+ adsorption/reaction is shown in **Figure 3b**. NH_4^+ adsorption and reaction with $MgCO_3$ followed a very similar behavior of that of PO_4^{3-} with 5 and 20 ppm Cu^{2+} precursor solutions not removing any NH_4^+ while $MgCO_3$ alone led to its complete removal. This suggests a facile removal of both nutrient ions in the presence of 100 ppm Zn^{2+} is possible albeit exhibiting a delayed formation reaction for ~25 minutes. Important data is shown in the concentration profiles of Mg^{2+} in solution as a function of reaction time in **Figure 3c** which showed that there was an immediate dissolution (mobilization) of Mg^{2+} ions from solid $MgCO_3$ within 5 min of the reaction. The initial fast dissolution was strongly inhibited in 100 ppm Zn^{2+} case for 25 min and the same equilibrium concentration of Mg^{2+} ions was achieved. An increase in the Mg^{2+} ion concentration agreed well with the increasing pH of the solution shown in **Figure 3d**. Here the initial 1000 ppm $NH_4H_2PO_4$ solution pH was ~4.4 and the first measurement with $MgCO_3$ added was taken 1-2 min after the addition. A quite remarkable was almost complete inhibition of Mg^{2+} ion release into solution when 20 ppm Cu^{2+} was present. Results show that while pH increased in all the cases of $MgCO_3$, pH reached a steady-state value of ~7. While struvite formation typically required a pH of 8.5,(12) present experiments and literature data suggest that bulk solution pH is not representative of the struvite formation conditions as the local pH on the $MgCO_3$ surface is likely higher.(19) Instead, low pH values of the solution should result in more Mg^{2+} dissolved, the phenomenon not observed for the 20 ppm

Cu^{2+} case. This suggests that low concentration of Cu^{2+} ions inhibits the initial transformation, likely dissolution of Mg^{2+} ion, from $MgCO_3$ surface necessary to form struvite, as opposed to the bulk solution pH driven transformations typically referred to in the literature. As supported by XRD data (*vide infra*), 100 ppm Zn^{2+} containing $NH_4H_2PO_4$ solution precipitates as zinc phosphate solid since its concentration is higher than that of Cu^{2+} and supersaturation can be achieved for phosphate to be the most favorable solid phase, especially in the initial stage of the reaction. Cu^{2+} concentrations used in these experiments do not lead to any detectable solid phases due to the absence of the supersaturation but rather Cu^{2+} ions adsorb on $MgCO_3$ surface as $Cu(OH)_2$ blocking Mg^{2+} from being released into solution, a condition needed to form struvite, as shown in **Figure 3c**. Importantly, a wide range of supporting experiments were performed using $MgCl_2$ as magnesium source at the molar amount equivalent to that of $MgCO_3$ in the presence of 20 ppm Cu^{2+} and in all cases struvite formation was observed.

The kinetics of phosphate adsorption were analyzed using the pseudo-first order (PFO) and the pseudo-second order (PSO) models as shown in **Figure 4a** and **b**, respectively. PSO is typically applicable when the absorbing species represents one reactant and the surface site is the second reactant while in the PFO model surface site is not part of the kinetic expression.(46–48) Hence, literature reports which utilized $MgCl_2$ as the magnesium source reported that first-order kinetics can be used for struvite crystallization with no transition metal ions present.(49,50) Conceptually, however, phosphate adsorption on solid $MgCO_3$ should follow PSO kinetics. However, previous reports that utilized $MgCO_3$ for struvite synthesis have shown that the PFO model shows higher R^2 fits (with no transition metals present in aqueous solution), e.g. mathematically it is also correct even though lacking physical meaning.(19) In this work, the $MgCO_3$ alone (no Cu^{2+} or Zn^{2+} present in the simulated wastewater solution) showed a higher R^2 value of 0.992 for the PFO model that 0.905 for PSO. One possible explanation for the PFO model showing high R^2 values compared to PSO in the case of phosphate adsorption on $MgCO_3$ could be that $MgCO_3$ has a higher solubility and thus, the surface restructuring steps required to adsorb phosphate may occur faster compared to adsorbents, such as MgO,(10,13,16,51) that exhibit true PSO type kinetic behavior. This is consistent with the data in **Figure 4a** and kinetics data observed in **Figure 3c** where Mg^{2+} is released into the bulk solution without but at increasingly slower rates when 5 ppm Cu^{2+} or 100 ppm Zn^{2+} are present. The addition of 5 ppm and 20 ppm Cu^{2+} did not result in high R^2 values, but due to the low phosphate adsorption in **Figure 3a**, this can be proposed due to the lack of struvite

formation. 100 ppm of Zn^{2+} resulted in a satisfactory R^2 value of 0.958 using both PFO as well as PSO kinetics. Hence, 100 ppm Zn^{2+} modified the reaction kinetics but did not inhibit struvite formation. Completely different was measured reaction kinetics in the presence of either 20 or 5 ppm of Cu^{2+} which resulted in poor either PFO or PSO fits. This suggested a significant inhibition effect of ppm concentrations of Cu^{2+} when $MgCO_3$ is used as a magnesium source. On contrary, literature reports showed that struvite crystallized in the presence of 5 ppm Cu^{2+} using $MgCl_2$ with the reported first-order rate constant of 3.58 h^{-1}, which showed that Cu^{2+} even at low concentrations inhibited struvite crystallization kinetics and an appreciable amount of solid struvite formed.(29) Interestingly, the same study(29) reported on struvite crystallization from $MgCl_2$ in the presence of Zn^{2+}, which showed similar results to Cu^{2+} where at low concentrations of 5 ppm, the reaction rates were similarly inhibited.

The Cu^{2+} and Zn^{2+} concentrations were measured as a function of time to understand the kinetics of metal adsorption on the solid phase and are shown in **Figure 5a**. Typically, metal ion adsorption from wastewater follows PSO kinetics.(52–54) Therefore, the concentration data for Cu^{2+} and Zn^{2+} was fitted to the PSO model as shown in **Figure 5b**. 5 and 20 ppm Cu^{2+} and 100 ppm Zn^{2+} experiments all fit the PSO model with R^2 values above 0.99, indicating that the PSO model is the correct approach to modeling the metal adsorption regardless the concentration or metal nature. This suggests metal ions adsorb on the heterogeneous $MgCO_3$ (even though they also were recently shown to be efficiently adsorbed by struvite(34)) surface with ~80% within the first 20 min of the reaction, suggesting the observed plateau in **Figure 3a** and **b** for both PO_4^{3-} and NH_4^+ in 100 ppm Zn^{2+} case is an initial reaction phase, likely through a solid zinc-containing intermediate. Similarly, fast initial adsorption of Cu^{2+} suggests not the gradual incorporation into the lattice but rather fast interaction with the $MgCO_3$ surface, potentially leading to its passivation against Mg^{2+} dissolution.

Figure 6 presents the elemental composition of the main metals, Mg, Cu, Zn, and and nonmetal P in the recovered filtered and dried solid precipitate as well as in the filtrate obtained from 20 ppm Cu^{2+} and 100 ppm Zn^{2+} containing wastewater transformation into struvite. Quite remarkably, all of the Zn^{2+} and most of the Cu^{2+} ions were incorporated into the resulting solid precipitate. Mg and P, on the other hand, partitioned between the solid and liquid phases quite differently. In the 20 ppm Cu^{2+} case almost all of the Mg accumulated in the solid phase while P was not absorbed,

consistent with ion chromatography measurements. In 100 ppm Zn^{2+} case, Mg partitioned between both solid and liquid phase where P was mostly retained in the solid. Collectively, these data show that small amounts of Cu^{2+} and Zn^{2+} ions can profoundly affect not only the formation kinetics of the struvite product but also completely inhibit PO_4^{3-} (and NH_4^+) adsorption/reaction on $MgCO_3$, a phenomenon not routinely observed when $MgCl_2$ was used even at relatively high metal ion concentrations.(29,35,55,56)

Solid-phase crystalline characterization of struvite formation products formed using $MgCO_3$. Motivated by the slow adsorption of PO_4^{3-} ions in the presence of Cu^{2+} observed, a range of struvite synthesis experiments was performed with 2, 5, 10 or 20 ppm Cu^{2+} to analyze the resulting crystalline nature of the precipitate. XRD results for Cu-struvite in **Figure 7** show that moderate concentrations of Cu^{2+} (10 and 20 ppm) in the wastewater precursor solution suppress struvite formation, while low concentrations of Cu^{2+} (5 ppm) lead to the onset of the struvite crystallization. In particular, the resulting XRD patterns when 10 and 20 ppm of Cu^{2+} were used are effectively very similar to those of the $MgCO_3$, as shown in **Figure 7a**. 100 ppm of Zn^{2+} also showed struvite phase formed after 2 hours but a distinct hopeite ($Zn_3(PO_4)_2{\cdot}4H_2O$) crystalline phase after the 20 minutes of reaction as shown in **Figure 7b**. This is in a good agreement with pseudo 2nd order kinetics observed for Zn^{2+} removal from simulated wastewater solution. The supporting EDS measurements are shown in **Figure 8** confirm the presence of Zn^{2+} in the solid phase after 20 min with less P incorporated than after 2-hour synthesis. It can also be seen that no P is incorporated into the reaction product when 20 ppm Cu^{2+} was used while in 5 ppm Cu^{2+} case elongated struvite crystals started appearing with dispersed copper.

The nature of copper sites in the solid precipitate is critical in this work as it can suggest potential green struvite fertilizer product biotoxicity. To understand the molecular arrangement of these sites, ambient XANES K-edge studies were conducted to elucidate the coordination for the Cu^{2+} and Zn^{2+} atomic centers incorporated into the synthesized solid precipitate. **Figure 9a** shows the 5 ppm and 20 ppm Cu^{2+} near-edge spectra with the references Cu_2O, CuO, and $CuSO_{4\,(aq)}$. The pre-edge feature of the Cu_2O which contains linearly coordinated Cu^{2+} is absent in both the 5 and 20 ppm samples. The minor feature at 8977 eV for $CuSO_4$ is observed on both 5 and 20 ppm Cu^{2+}. This feature has been previously reported in the literature as the 1s → 3d transition.(57) The lack of a pre-edge feature indicates Cu^{2+} to be in symmetric coordination, similar to CuO (square

planar) $CuSO_{4\,(aq)}$ (elongated octahedral). The white line of both 5 and 20 ppm samples align with CuO and $CuSO_4$, indicating the majority of Cu sites are in the 2+ oxidation state (but not in oxide form). **Figure 9b** shows the XANES for Zn-struvite and the reference ZnO spectrum. The shift in the main edge feature which is attributed to 1s → 4p(58) indicates distortion from the ZnO structure. The smaller peak following the main edge is attributed to multiple scattering resonance.(59) The ZnO reference and 100 ppm Zn^{2+} spectra show significant differences, indicating that Zn^{2+} exists in a disordered phosphate-hydrate phase.(60–62) The XANES spectra bear similarity to hopeite (as discussed earlier in XRD findings), while EXAFS shows that Zn has a distorted octahedral local coordination.

The ambient K-edge EXAFS studies were conducted to elucidate the nearest neighbor information. Table 1 shows the bond length (R), coordination number (N), mean square variation in path length (σ^2), and R factor for the fit. In all three cases, only a single shell is observed, which indicates that the metal centers only have short-range order and show no long-range order given the lack of Me-O-Me bridging bonds. The 5 ppm and 20 ppm Cu^{2+} EXAFS spectra were fitted with N = 4 for equatorial O and N = 2 for axial O bonds. The longer equatorial bond distances were calculated with higher error in fit compared to the equatorial O bond lengths. XANES analysis indicates that Cu^{2+} is coordinated to O in symmetrical coordination and given the elongated Cu-O axial bond it is difficult to determine whether the exact coordination is square planar or elongated octahedral. In the case of 100 ppm Zn^{2+}, three models were evaluated. The lowest R factor was found to be Zn^{2+} coordinated to 4 equatorial O and 2 axial O atoms. Between the N = 4 model and the N = 4 and 2 model the R factor variation is minor and thus, it is difficult to discriminate between the models without further experimental evidence to prove the exact Zn^{2+} coordination. However, EXAFS analysis conclusively proves that all transition metal centers are highly isolated in the struvite structure, which contrasts from work done using $MgCl_2$ where polymeric Zn^{2+} was detected.(32)

Table 1. EXAFS fitting parameters for reaction products of 1000 ppm $MgCO_3$ and 1000 ppm MAP in the presence of 5 and 20 ppm Cu^{2+} and 100 ppm Zn^{2+}.

Sample	Path	N	R (Å)	σ^2 (Å^2)	R Factor (%)
5 ppm Cu^{2+}	Cu-O (eq.)	4	1.940 (0.009)	0.0050 (0.0006)	1.8

	Cu-O (ax.)	2	2.5 (0.1)	0.037 (0.022)	
20 ppm Cu^{2+}	Cu-O (eq.)	4	1.939 (0.090)	0.0058 (.0005)	1.9
	Cu-O (ax.)	2	2.5 (0.1)	0.035 (0.025)	
100 ppm Zn^{2+}	Zn-O	6	1.967 (0.021)	0.0179 (0.0014)	5.8
	Zn-O	4	1.972 (0.010)	0.0113 (0.0007)	2.1
	Zn-O	4	1.993 (0.010)	0.0098 (0.0006)	1.7
		2	2.27 (0.02)	0.017 (0.004)	

Furthermore, EXAFS analysis showed that copper metal centers exist in disordered form, which agrees with previous reports.(33) A previous study demonstrated that particle size effects exist (micro vs nano) for Cu^{2+} uptake in plants. The study concluded that microparticles inhibited root growth at a higher level compared to nanoparticles.(63) Cu-struvite has been characterized as a potential slow-release fertilizer for micronutrient delivery in a previous report(64) with copper precipitation occurring as both phosphate and hydroxide phases. It was shown that organic acids secreted by root systems assisted in forming soluble Cu^{2+} species in soil that can be readily taken up by the plants. The data shown in **Figure 10** suggest that Cu^{2+} species are coordinated differently from those of bulk corresponding oxides (Cu_2O and CuO) and exhibit octahedral coordination.(65)

The Zn-struvite showed minor additional peaks for the 2-hour product in XRD data in **Figure 7**, notably at 9.76° which may be attributed to a $Zn_3(PO_4)_2{\cdot}4H_2O$ (hopeite) minor product formation along with the struvite major product. As shown by EXAFS analysis, the Zn^{2+} metal centers exist without long-range order, indicating an amorphous (or disordered) phase.(61) Struvite formed using $MgCl_2$ has also been shown to have similar Zn^{2+} centers at low zinc concentrations.(32)

Struvite effects on biomass

Soil microbial biomass carbon (SMBC) response to struvite synthesis solid precipitate. Preceding discussion suggests that synthesized precipitate contains both Zn and Cu when using solid $MgCO_3$ as a magnesium source. Soil microbial biomass is often used as an early indicator of soil quality changes and is susceptible to changes in the soil environment and soil environmental practices.(66,67) The rapid increase in biomass over the first 12 days (**Figure 11a**) of incubation in the struvite treatment indicates that it is a suitable N source for aerobic microbial growth and

the release of CO_2.(68) The initial increase observed in both the struvite and struvite obtained from simulated wastewater solutions containing Zn^{2+} 100 ppm biomass is consistent with N-fertilization in a nitrogen-limited environment. The lack of increased biomass in the struvite from 20 ppm Cu^{2+} containing wastewater indicates an overall growth-limiting effect that can be associated with copper toxicity and is consistent with previous studies that have shown copper inhibition of soil microbial biomass C.(69,70) After 12 days of incubation the struvite treatment resulted in an overall reduction of the biomass compared to the control. This reduction could be due to the rapid depletion of O_2 caused by increased respiration resulting from N-fertilization and a transition from consortia dominated by aerobic organisms to anaerobic. However, biomass continued to increase in the control and struvite made from 100 ppm Zn^{2+} containing wastewater treatments until 28 days followed by a reduction in biomass to the same level as the struvite synthesized from simulated wastewater containing 100 ppm Zn^{2+} at 48 days. The presence of the zinc may have slowed the growth of the microbial biomass compared to struvite and simply resulted in a delay in the onset of anaerobic conditions. Alternatively, the presence of the zinc may have led to increased alcohol dehydrogenase activity as the consortia became more anaerobic resulting in increased growth in facultative anaerobic organisms. The control treatment was already at a steady-state with regards to N content so there was no increased respiration resulting in a much longer lag time until the onset of anaerobic conditions and the commensurate reduction in anaerobic biomass.

Dehydrogenase activity helps to access the enzymatic activity in the soil and serves as an indicator of microbiological redox systems and is closely correlated with respiratory (aerobic) activity in the soil.(71) Soil dehydrogenase activity was greatly influenced by the addition of N as shown in **Figure 11b**. This was evidenced by the significant decrease in DHA through the incubation period. DHA reduction in the struvite and struvite synthesized using 100 ppm Zn^{2+} containing model wastewater are indicative of a transition from aerobic to anaerobic conditions over the first 12 days of incubation and are consistent with the biomass data. The TTC method used to measure DHA is not suited to measure anaerobic dehydrogenase so the level indicated is probably representative of the equilibrium redox state reached after 12 days. Metal concentrations tend to directly affect enzyme activity rather than microbial biomass reduction. The rapid reduction in DHA observed in the struvite synthesized using 20 ppm Cu^{2+} containing wastewater would indicate that there is an overall negative or toxic effect due to the copper. This confirmed studies

by(72,73) stating inhibition of enzymatic activity in soils by changing the microflora composition and activity of individual enzymes which decreases organic matter decomposition. One possible explanation for the slight increase in DHA in struvite on day 28 may be a result of an increase in pH based on the application of struvite which confirms previous reports that changes in pH of the soil are a frequent effect of struvite application.(14,74) The increased pH has a direct effect on dehydrogenase activity as also reported by other authors.(75)

The activity of soil microorganisms strongly depends on the presence of available organic C and N. The lower microbial activity observed in the amendments compared to control may partly be attributed to the quality and as well as the complex interaction of the amendments with the soil.(76) The alkaline state of the soil makes initial solubility lower in struvite and other amendments hence did not stimulate quicker mineralization of available soil nutrients (phosphorus forms) and a faster growth rate of the soil microorganisms. The lower solubility can be assumed to result in a greater immobilization of P compared to the mineralization of the available organic compounds. This resulted in the moderate to low soil microbial-mediated mineralization in struvite, and that obtained using 100 ppm Zn^{2+} and 20 ppm Cu^{2+} containing model wastewater as evidenced by the positive correlation between the DHA and SMB-C shown in **Figure 11c**.

Conclusions and Environmental Implications. Struvite synthesis using N and P available in wastewater requires a magnesium source which can be either water-soluble $MgCl_2$ or very low water solubility but more available magnesium minerals, including $MgCO_3$. $MgCl_2$ is produced via energy-demanding processes while $MgCO_3$ is an abundant mined mineral(10) suggesting its use can be beneficial for low environmental impact nutrient recovery process. However, the data presented in this work show that the nature of the complex wastewater needs to be carefully considered before $MgCO_3$ can be used to substitute for $MgCl_2$. In particular, while solid struvite formed from the simulated wastewater with and without 100 ppm Zn^{2+}, already ppm-level concentrations of Cu^{2+} inhibited the formation of crystalline struvite. The likely mechanism for this phenomenon was surface adsorption of Cu^{2+} ions on $MgCO_3$ which inhibited Mg^{2+} ion release from the surface. This is an interesting observation and the exact mechanism is a subject of a detailed surface science study. Notably, this negative effect of the Cu^{2+} ions on the formation of struvite was not observed when $MgCl_2$ was used as magnesium source for a wide range of Cu^{2+}

ion concentrations.(29,33,55,56) These surface adsorbed Cu^{2+} sites exhibited a strong effect on soil biota, likely due to being more mobile or soluble. This phenomenon was not observed when 100 ppm Zn^{2+} was present in the simulated wastewater. The Zn-struvite formation proceeded via a formation of $Zn_3(PO_4)_2{\cdot}4H_2O$ intermediate in the first ~25 minutes of the reaction which led to disordered or amorphous Zn local structure in the final product. Notably, in either case, the parent $MgCO_3$ was a very efficient metal ion adsorbent with both transition metals very efficiently adsorbed and concentrated in the resulting solid under the reaction conditions considered. This suggests that when a more sustainable Mg^{2+} source based on low solubility Mg minerals is considered, due attention needs to be given to the abundance of the particular transition metals in the wastewater.

CRediT author statements. Karolina Barčauskaitė: Investigation and writing the original draft. **Donata Drapanauskaitė:** Investigation. **Manoj Silva:** Visualization, data curation and writing the original draft. **Vadim Murzin:** Investigation. **Modupe Doyeni:** Investigation. **Marius Urbonavicius:** Investigation. **Clinton F. Williams:** Data curation. **Skaidrė Supronienė:** Investigation. **Jonas Baltrusaitis:** Conceptualization, supervision, writing review & editing.

Conflicts of interest. There are no conflicts of interest to declare.

Acknowledgments. This material is based upon work supported by the National Science Foundation under Grant No. CHE 1710120. VM is grateful for financial support from the BMBF project 05K19PXA.

Figures:

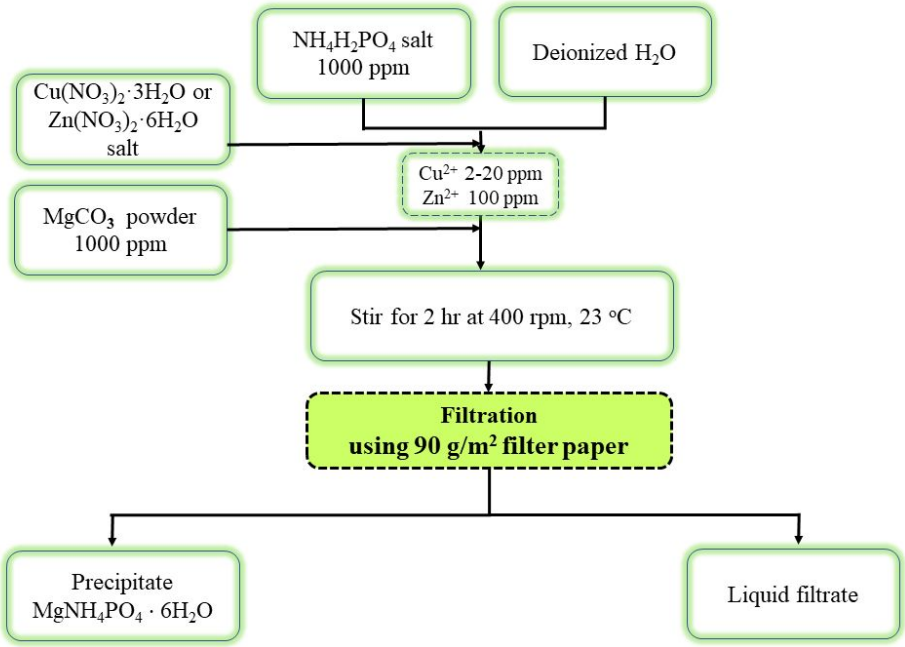

Figure 1. Experimental procedure for struvite synthesis with and without Cu^{2+} and Zn^{2+} in simulated wastewater.

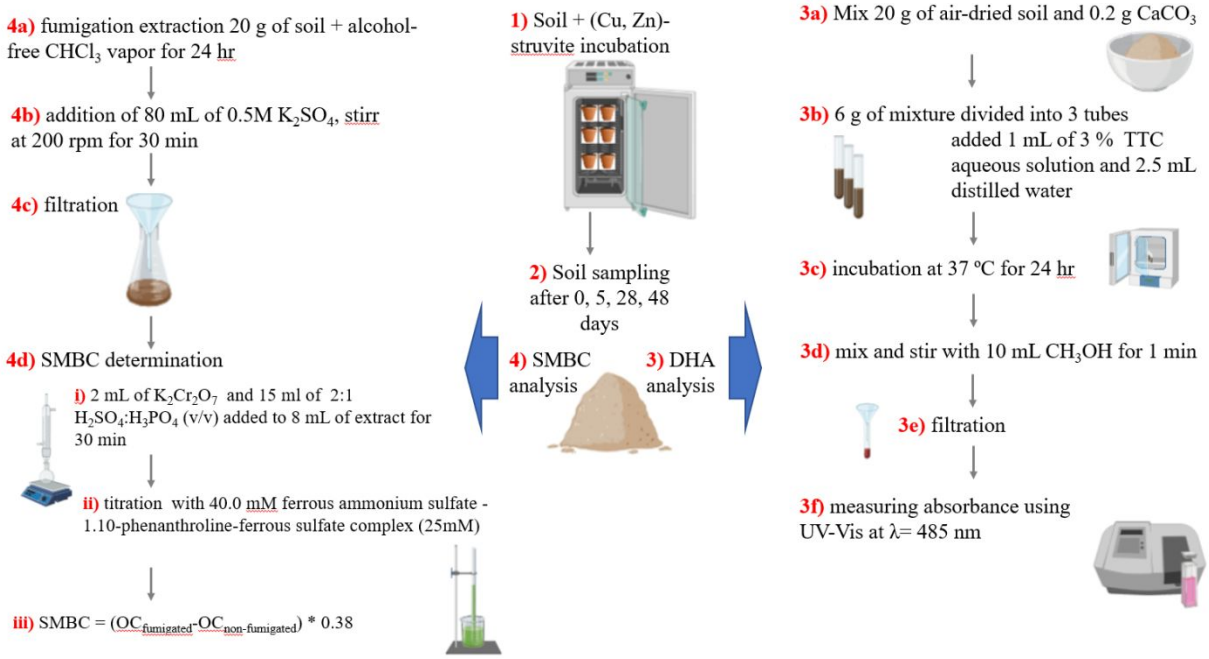

Figure 2. Experimental procedure for SMBC and DHA analysis.

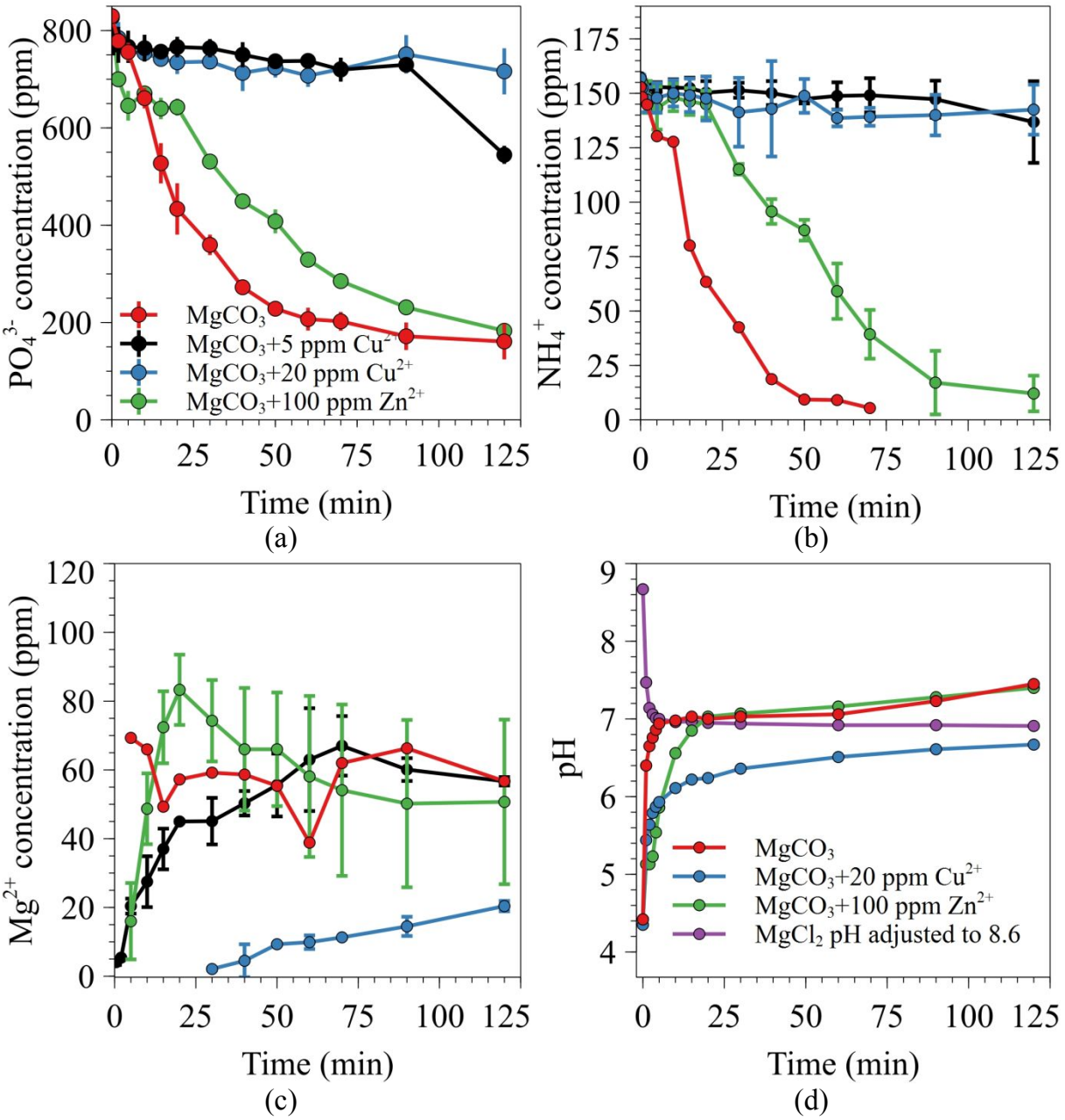

Figure 3. Measured temporal profiles of (a) PO_4^{3-}, (b) NH_4^+, (c) Mg^{2+} during struvite formation using 1000 ppm $MgCO_3$ and 1000 pm MAP. (d) pH change as a function of reaction time, after addition of 1000 ppm $MgCO_3$ with 1000 MAP. 5, 20 ppm Cu^{2+} or 100 ppm Zn^{2+} were also used in simulated wastewater. In (d) temporal pH profile of $MgCl_2$ with the initial pH adjusted to 8.6 is also shown for comparison. Error bars in (a), (b) and (c) represent three independent measurements.

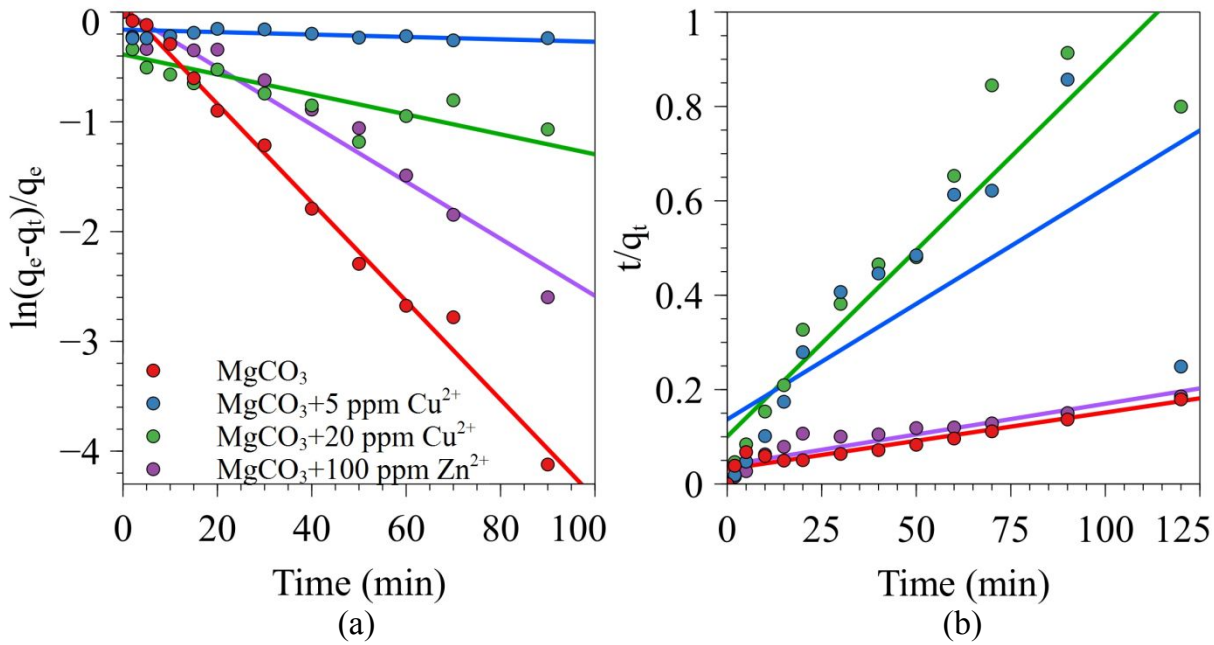

Sample	R^2	
	PFO	PSO
$MgCO_3$	0.992	0.905
$MgCO_3$+Cu^{2+} 5 ppm	0.201	0.470
$MgCO_3$+Cu^{2+} 20 ppm	0.671	0.879
$MgCO_3$+Zn^{2+} 100 ppm	0.958	0.834

Figure 4. Kinetic modeling of total PO_4^{3-} experimental data using (a) pseudo 1st order and (b) pseudo 2nd order kinetics model for 1000 ppm $MgCO_3$ and 1000 ppm MAP with and without 5, 20 ppm Cu^{2+} or 100 ppm Zn^{2+}.

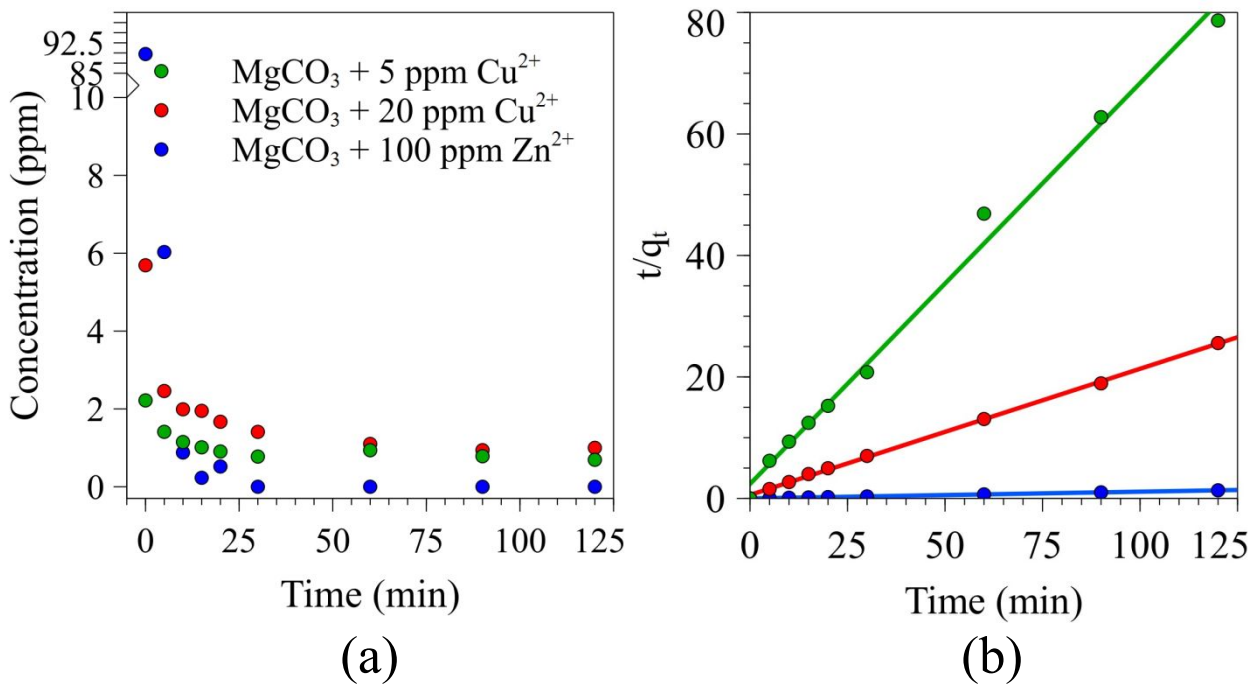

Figure 5. (a) Measured temporal profiles of Cu^{2+} and Zn^{2+} during struvite formation using 1000 ppm $MgCO_3$ and 1000 ppm MAP with 5, 20 ppm Cu^{2+} or 100 ppm Zn^{2+} added in the simulated wastewater solution. (b) Kinetic modeling of experimental data using pseudo 2nd order kinetics model for 5, 20 ppm Cu^{2+} or 100 ppm Zn^{2+} .

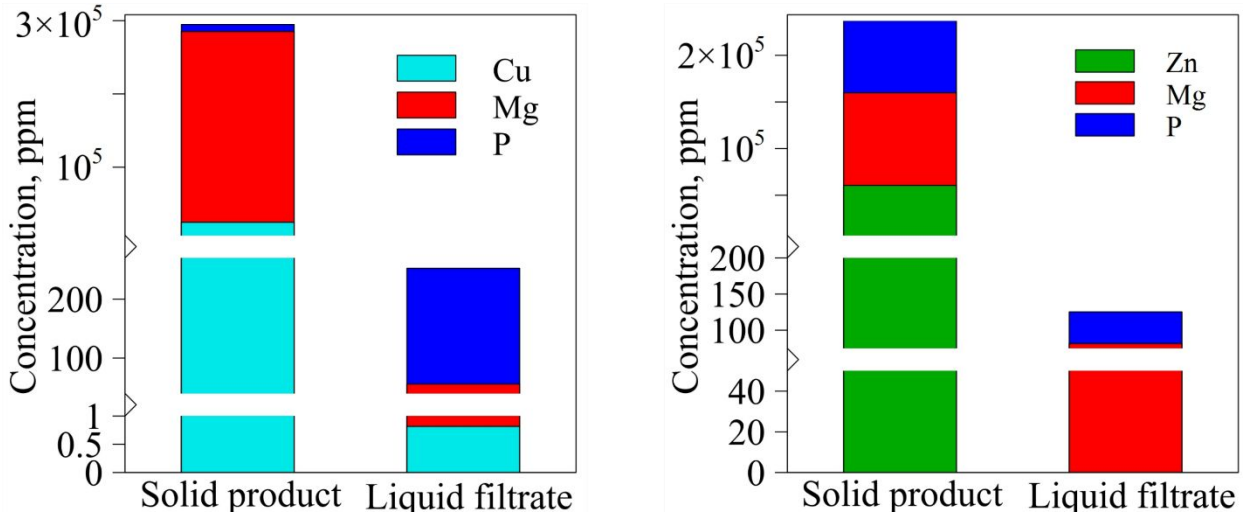

Figure 6. (a) ICP measured Cu(Zn), Mg and P concentrations in solid precipitate and the liquid filtrate for 20 ppm Cu^{2+} and 100 ppm Zn^{2+}.

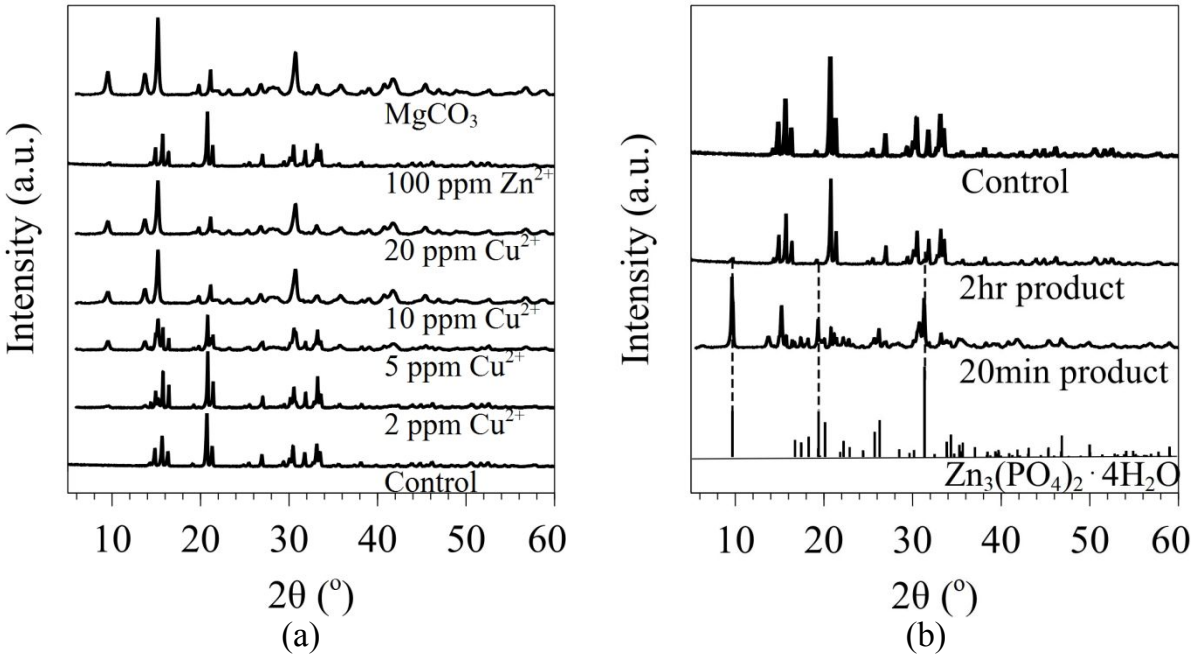

Figure 7. XRD patterns measured of various struvite formation solid precipitate using $MgCO_3$ with and without Cu^{2+} or Zn^{2+} in the simulated wastewater solution. Control represent struvite formed with no metals added.

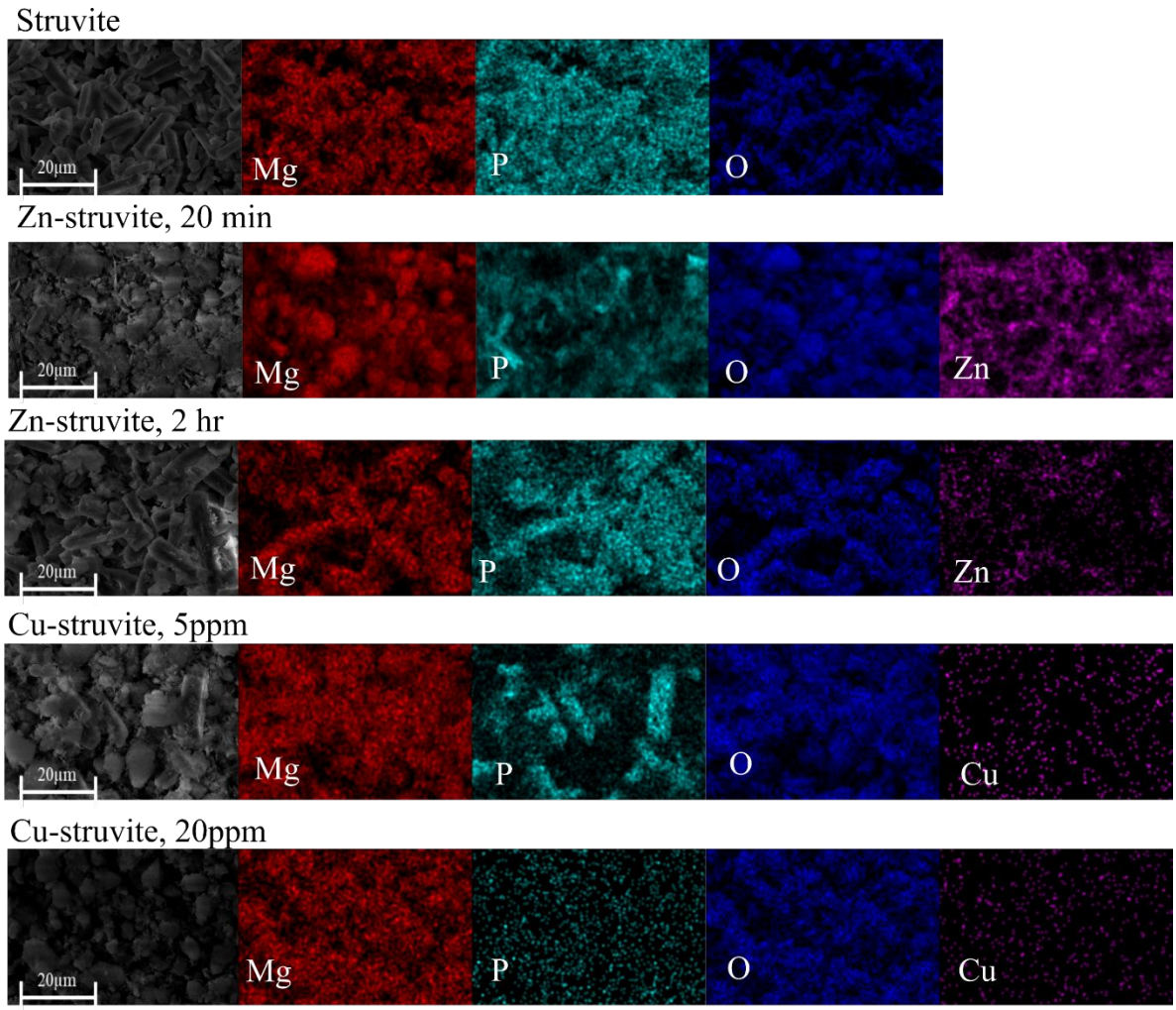

Figure 8. SEM images together with the elemental EDS maps of various struvite formation solid precipitate using $MgCO_3$ with and without Cu^{2+} or Zn^{2+} in the simulated wastewater solution.

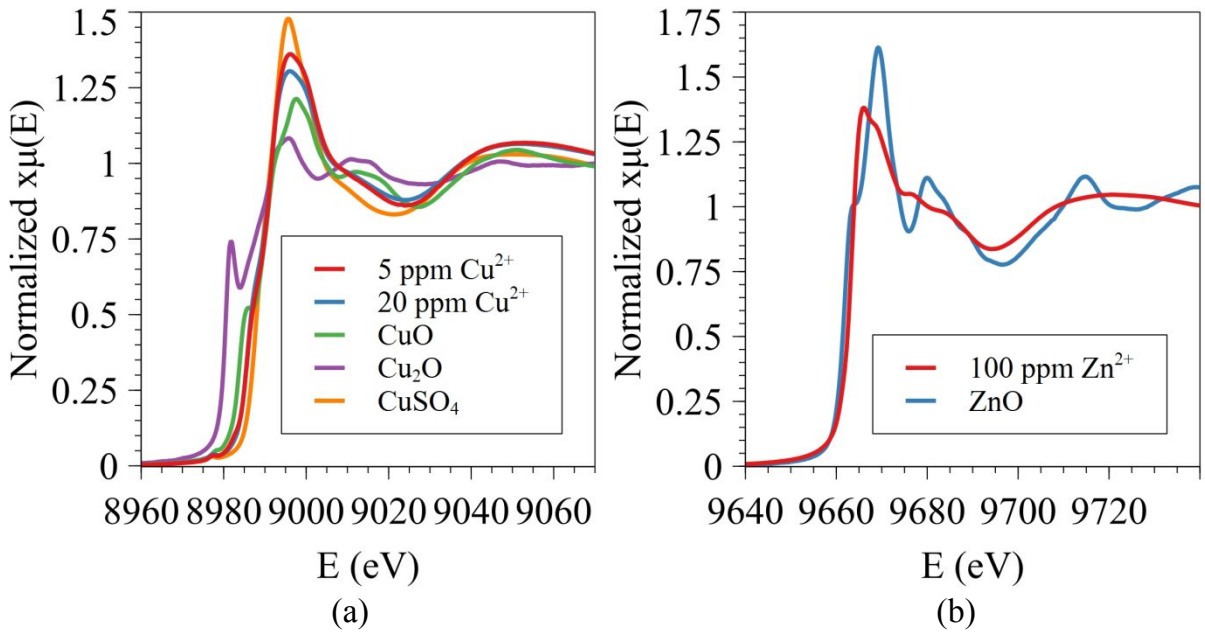

Figure 9. (a) Cu K-edge XANES for Cu 5 ppm and Cu 20 ppm samples with Cu_2O, CuO, and $CuSO_4$ reference spectra (b) Zn K-edge XANES for Zn sample with ZnO reference spectrum.

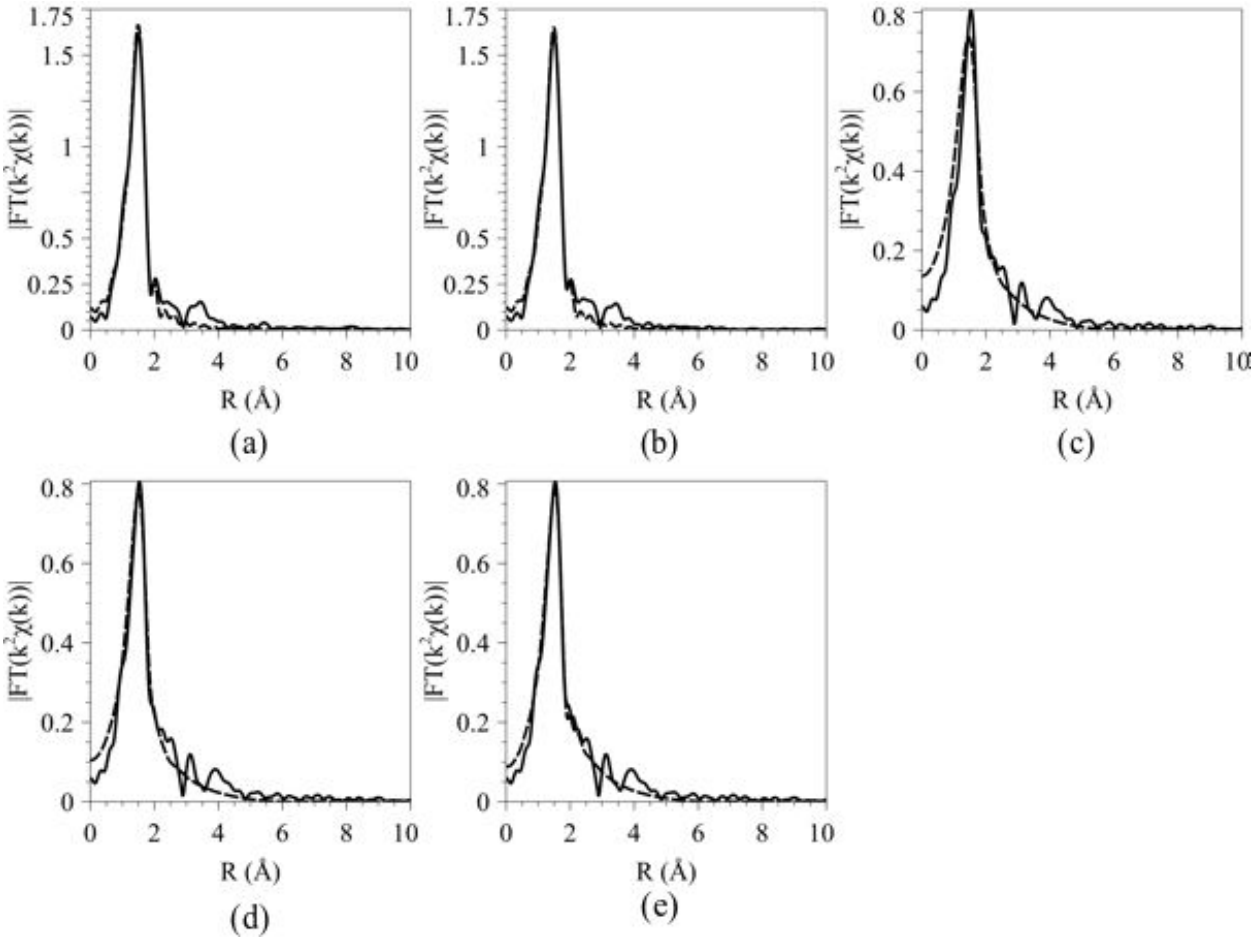

Figure 10. (a) Cu-K-edge EXAFS for Cu 5 ppm (b) Cu K-edge EXAFS for 20 ppm Cu^{2+} (c) Zn K-edge EXAFS for 100 ppm Zn^{2+} (fit N = 6) (d) Zn K-edge EXAFS for 100 ppm Zn^{2+} (fit N = 4) (e) Zn K-edge EXAFS for 100 ppm Zn^{2+} (fit N = 4 and 2). The solid line denotes experimental spectrum, and the dashed line denotes the fitted model.

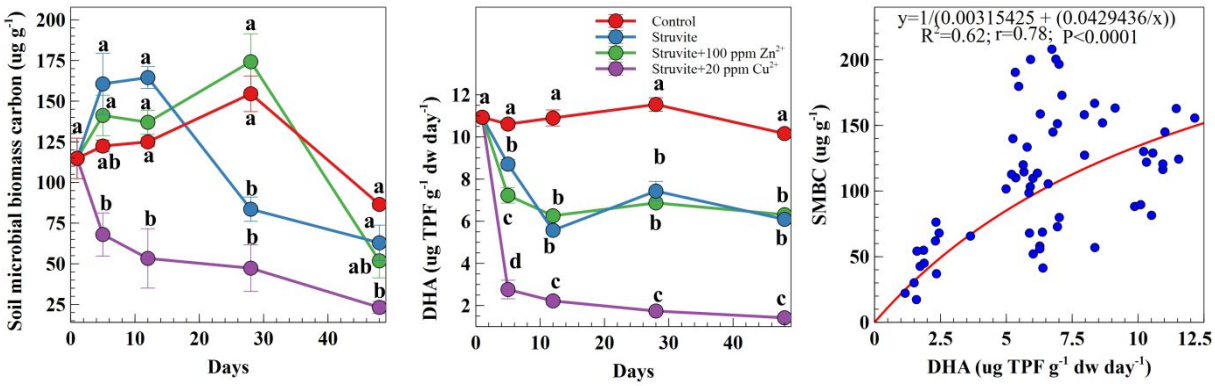

(a) (b) (c)

Figure 11. (a) Soil microbial biomass carbon (SMBC) content and (b) soil DHA activity and (c) the correlation between SMBC and DHA. The best fit is a double reciprocal correlation curve which explains 61.59 % of the obtained results. The correlation coefficient (r=0.78) indicates that there is a strong positive relationship between SMBC and DHA values.

References

1. Bouwman L, Goldewijk KK, Van Der Hoek KW, Beusen AHW, Van Vuuren DP, Willems J, et al. Exploring global changes in nitrogen and phosphorus cycles in agriculture induced by livestock production over the 1900–2050 period. Proc Natl Acad Sci [Internet]. 2013 Dec 24;110(52):20882 LP – 20887. Available from: http://www.pnas.org/content/110/52/20882.abstract

2. Bouwman AF, Boumans LJM, Batjes NH. Estimation of global NH_3 volatilization loss from synthetic fertilizers and animal manure applied to arable lands and grasslands. Global Biogeochem Cycles. 2002 Jun;16(2):8-1-8–14.

3. Galloway JN, Aber JD, Erisman JW, Seitzinger SP, Howarth RW, Cowling EB, et al. The Nitrogen Cascade. Bioscience [Internet]. 2003 Apr 1;53(4):341–56. Available from: http://dx.doi.org/10.1641/0006-3568(2003)053[0341:TNC]2.0.CO

4. Baltrusaitis J. Sustainable Ammonia Production. ACS Sustain Chem Eng. 2017;5(11):9527–9527.

5. Cordell D, Rosemarin A, Schröder JJ, Smit AL. Towards global phosphorus security: a systems framework for phosphorus recovery and reuse options. Chemosphere [Internet]. 2011 Aug [cited 2014 Jul 10];84(6):747–58. Available from: http://www.sciencedirect.com/science/article/pii/S0045653511001652

6. Cordell D, Drangert J-O, White S. The story of phosphorus: Global food security and food for thought. Glob Environ Chang. 2009 May;19(2):292–305.

7. Zhang H., Cao Z., Shen Q., Wong M. Effect of phosphate fertilizer application on phosphorus (P) losses from paddy soils in Taihu Lake Region: I. Effect of phosphate fertilizer rate on P losses from paddy soil. Chemosphere. 2003 Feb;50(6):695–701.

8. Mazzei L, Broll V, Casali L, Silva M, Braga D, Grepioni F, et al. Multifunctional Urea Cocrystal with Combined Ureolysis and Nitrification Inhibiting Capabilities for Enhanced Nitrogen Management. ACS Sustain Chem Eng [Internet]. 2019 Jul 18;acssuschemeng.9b02607. Available from: https://doi.org/10.1021/acssuschemeng.9b02607

9. Casali L, Mazzei L, Shemchuk O, Sharma L, Honer K, Grepioni F, et al. Novel Dual-Action Plant Fertilizer and Urease Inhibitor: Urea·Catechol Cocrystal. Characterization and Environmental Reactivity. ACS Sustain Chem Eng [Internet]. 2019 Jan 22;7(2):2852–9. Available from: https://doi.org/10.1021/acssuschemeng.8b06293

10. Kiani D, Sheng Y, Lu B, Barauskas D, Honer K, Jiang Z, et al. Transient Struvite Formation during Stoichiometric (1:1) NH4+ and PO43– Adsorption/Reaction on Magnesium Oxide (MgO) Particles. ACS Sustain Chem Eng. 2018;7:1545–56.

11. Sharma L, Kiani D, Honer K, Baltrusaitis J. Mechanochemical Synthesis of Ca- and Mg-Double Salt Crystalline Materials Using Insoluble Alkaline Earth Metal Bearing Minerals. ACS Sustain Chem Eng. 2019;7:6802–12.

12. Le Corre KS, Valsami-Jones E, Hobbs P, Parsons SA. Phosphorus Recovery from Wastewater by Struvite Crystallization: A Review. Crit Rev Environ Sci Technol. 2009 Jun;39(6):433–77.

13. Kiani D, Silva M, Sheng Y, Baltrusaitis J. Experimental Insights into the Genesis and Growth of Struvite Particles on Low-Solubility Dolomite Mineral Surfaces. J Phys Chem C [Internet]. 2019 Oct 17;123(41):25135–45. Available from: https://pubs.acs.org/doi/10.1021/acs.jpcc.9b05292

14. Talboys PJ, Heppell J, Roose T, Healey JR, Jones DL, Withers PJA. Struvite: a slow-release fertiliser for sustainable phosphorus management? Plant Soil [Internet]. 2016;401(1):109–23. Available from: https://doi.org/10.1007/s11104-015-2747-3

15. Silva M, Barcauskaite K, Drapanauskaite D, Tian H, Bučko T, Baltrusaitis J. Relative Humidity Facilitated Urea Particle Reaction with Salicyclic Acid: A Combined in situ Spectroscopy and DFT Study. ACS Earth Sp Chem. 2020 Jun;

16. Xia P, Wang X, Wang X, Song J, Wang H, Zhang J, et al. Struvite crystallization combined adsorption of phosphate and ammonium from aqueous solutions by mesoporous MgO–loaded diatomite. Colloids Surfaces A Physicochem Eng Asp [Internet]. 2016 Oct 5;506:220–7. Available from: http://www.sciencedirect.com/science/article/pii/S092777571630440X

17. Quintana M, Sánchez E, Colmenarejo MF, Barrera J, García G, Borja R. Kinetics of phosphorus removal and struvite formation by the utilization of by-product of magnesium oxide production. Chem Eng J. 2005 Jul;111(1):45–52.

18. Stolzenburg P, Capdevielle A, Teychené S, Biscans B. Struvite precipitation with MgO as a precursor: Application to wastewater treatment. Chem Eng Sci [Internet]. 2015 Sep 8;133:9–15. Available from: http://www.sciencedirect.com/science/article/pii/S0009250915001797

19. Lu B, Kiani D, Taifan W, Barauskas D, Honer K, Zhang L, et al. Spatially Resolved Product Speciation during Struvite Synthesis from Magnesite (MgCO 3) Particles in Ammonium (NH 4 +) and Phosphate (PO 4 3–) Aqueous Solutions. J Phys Chem C [Internet]. 2019 Apr 11;123(14):8908–22. Available from: https://doi.org/10.1021/acs.jpcc.8b12252

20. Kirinovic E, Leichtfuss AR, Navizaga C, Zhang H, Christus JDS, Baltrusaitis J. Spectroscopic and microscopic identification of the reaction products and intermediates during the struvite (MgNH4PO4·6H2O) formation from magnesium oxide (MgO) and magnesium carbonate (MgCO3) microparticles. ACS Sustain Chem Eng. 2017;5(2):1567–77.

21. Hövelmann J, Putnis C V. In Situ Nanoscale Imaging of Struvite Formation during the Dissolution of Natural Brucite: Implications for Phosphorus Recovery from Wastewaters. Environ Sci Technol [Internet]. 2016 Dec 6;50(23):13032–41. Available from: http://dx.doi.org/10.1021/acs.est.6b04623

22. Pesonen J, Myllymäki P, Tuomikoski S, Vervecken G, Hu T, Prokkola H, et al. Use of Calcined Dolomite as Chemical Precipitant in the Simultaneous Removal of Ammonium

and Phosphate from Synthetic Wastewater and from Agricultural Sludge. ChemEngineering. 2019 Apr;3(2):40.

23. Chen L, Zhou CH, Zhang H, Tong DS, Yu WH, Yang HM, et al. Capture and recycling of ammonium by dolomite-aided struvite precipitation and thermolysis. Chemosphere. 2017 Nov;187:302–10.

24. Gupta VK, Ali I, Saleh TA, Nayak A, Agarwal S. Chemical treatment technologies for waste-water recycling - An overview. RSC Adv. 2012;2(16):6380–8.

25. Canziani R, Spinosa L. Sludge from wastewater treatment plants. In: Industrial and Municipal Sludge: Emerging Concerns and Scope for Resource Recovery. Elsevier; 2019. p. 3–30.

26. Jiries AG, Al Nasir FM, Beese F. Pesticide and heavy metals residue in wastewater, soil and plants in wastewater disposal site near Al-Lajoun Valley, Karak/Jordan. Water Air Soil Pollut. 2002;133(1–4):97–107.

27. Wang C, Hu X, Chen ML, Wu YH. Total concentrations and fractions of Cd, Cr, Pb, Cu, Ni and Zn in sewage sludge from municipal and industrial wastewater treatment plants. J Hazard Mater. 2005 Mar;119(1–3):245–9.

28. Zubala T, Patro M, Boguta P. Variability of zinc, copper and lead contents in sludge of the municipal stormwater treatment plant. Environ Sci Pollut Res. 2017 Jul;24(20):17145–52.

29. Muryanto S, Bayuseno AP. Influence of Cu2+ and Zn2+ as additives on crystallization kinetics and morphology of struvite. Powder Technol. 2014;253:602–7.

30. Ronteltap M, Maurer M, Gujer W. The behaviour of pharmaceuticals and heavy metals during struvite precipitation in urine. Water Res. 2007 May;41(9):1859–68.

31. Uysal A, Yilmazel YD, Demirer GN. The determination of fertilizer quality of the formed struvite from effluent of a sewage sludge anaerobic digester. J Hazard Mater. 2010 Sep;181(1–3):248–54.

32. Rouff AA, Juarez KM. Zinc Interaction with Struvite During and After Mineral Formation. Environ Sci Technol. 2014 Jun;48(11):6342–9.

33. Rouff AA, Ramlogan M V., Rabinovich A. Synergistic Removal of Zinc and Copper in Greenhouse Waste Effluent by Struvite. ACS Sustain Chem Eng. 2016 Mar;4(3):1319–27.

34. Tang C, Liu Z, Peng C, Chai L-Y, Kuroda K, Okido M, et al. New insights into the interaction between heavy metals and struvite: Struvite as platform for heterogeneous nucleation of heavy metal hydroxide. Chem Eng J [Internet]. 2019 Jun;365:60–9. Available from: https://linkinghub.elsevier.com/retrieve/pii/S1385894719302578

35. Peng C, Chai L, Tang C, Min X, Song Y, Duan C, et al. Study on the mechanism of copper–ammonia complex decomposition in struvite formation process and enhanced ammonia and copper removal. J Environ Sci [Internet]. 2017 Jan;51:222–33. Available from: https://linkinghub.elsevier.com/retrieve/pii/S100107421630242X

36. Ahmed N, Shim S, Won S, Ra C. Struvite recovered from various types of wastewaters:

Characteristics, soil leaching behaviour, and plant growth. L Degrad Dev. 2018;29(9):2864–79.

37. Gupta SK, Roy S, Chabukdhara M, Hussain J, Kumar M. Risk of metal contamination in agriculture crops by reuse of wastewater: An ecological and human health risk perspective. In: Water Conservation, Recycling and Reuse: Issues and Challenges. Springer Singapore; 2019. p. 55–79.

38. Cai T, Park SY, Li Y. Nutrient recovery from wastewater streams by microalgae: Status and prospects. Renew Sustain Energy Rev [Internet]. 2013;19:360–9. Available from: http://www.sciencedirect.com/science/article/pii/S1364032112006429

39. Caliebe WA, Murzin V, Kalinko A, Görlitz M. High-flux XAFS-beamline P64 at PETRA III. In: AIP Conference Proceedings. American Institute of Physics Inc.; 2019. p. 060031.

40. Ravel B, Newville M. ATHENA, ARTEMIS, HEPHAESTUS: Data analysis for X-ray absorption spectroscopy using IFEFFIT. In: Journal of Synchrotron Radiation. 2005. p. 537–41.

41. Newville M. EXAFS analysis using FEFF and FEFFIT. J Synchrotron Radiat. 2001 Mar;8(2):96–100.

42. Ankudinov A, Rehr J. Relativistic calculations of spin-dependent x-ray-absorption spectra. Phys Rev B - Condens Matter Mater Phys. 1997 Jul;56(4):R1712–6.

43. Casida LE, Klein DA, Santoro T. Soil dehydrogenase activity. Vol. 98, Soil Science. 1964. p. 371–6.

44. Vance ED, Brookes PC, Jenkinson DS. An extraction method for measuring soil microbial biomass C. Soil Biol Biochem. 1987 Jan;19(6):703–7.

45. Wu J, O'donnell AG, He ZL, Syers JK. Fumigation-extraction method for the measurement of soil microbial biomass-S. Soil Biol Biochem. 1994 Jan;26(1):117–25.

46. Azizian S. Kinetic models of sorption: A theoretical analysis. J Colloid Interface Sci. 2004 Aug;276(1):47–52.

47. Rudzinski W, Plazinski W. Kinetics of solute adsorption at solid/solution interfaces: A theoretical development of the empirical pseudo-first and pseudo-second order kinetic rate equations, based on applying the statistical rate theory of interfacial transport. J Phys Chem B. 2006 Aug;110(33):16514–25.

48. Rudzinski W, Plazinski W. Studies of the kinetics of solute adsorption at solid/solution interfaces: On the possibility of distinguishing between the diffusional and the surface reaction kinetic models by studying the pseudo-first-order kinetics. J Phys Chem C. 2007 Oct;111(41):15100–10.

49. Priharyoto Bayuseno A, Perwitasari DS, Muryanto S, Tauviqirrahman M, Jamari J. Kinetics and morphological characteristics of struvite (MgNH 4 PO 4 .6H 2 O) under the influence of maleic acid. Heliyon. 2017;e03533.

50. Rahaman MS, Ellis N, Mavinic DS. Effects of various process parameters on struvite

precipitation kinetics and subsequent determination of rate constants. Water Sci Technol. 2008 Apr;57(5):647–54.

51. Meshkani F, Rezaei M. Facile synthesis of nanocrystalline magnesium oxide with high surface area. Powder Technol. 2009 Nov;196(1):85–8.

52. Treto-Suárez MA, Prieto-García JO, Mollineda-Trujillo Á, Lamazares E, Hidalgo-Rosa Y, Mena-Ulecia K. Kinetic study of removal heavy metal from aqueous solution using the synthetic aluminum silicate. Sci Rep. 2020 Dec;10(1):1–12.

53. Peng W, Li H, Liu Y, Song S. A review on heavy metal ions adsorption from water by graphene oxide and its composites. Vol. 230, Journal of Molecular Liquids. Elsevier B.V.; 2017. p. 496–504.

54. Liu X, Song K, Liu W, Xiong Y, Xu Y, Shi Z, et al. Removal and recovery of Pb from wastewater through a reversible phase transformation process between nano-flower-like Mg(OH) 2 and soluble Mg(HCO 3) 2. Environ Sci Nano. 2019 Feb;6(2):467–77.

55. Perwitasari DS, Muryanto S, Jamari J, Bayuseno AP. Kinetics and morphology analysis of struvite precipitated from aqueous solution under the influence of heavy metals: Cu2+, Pb2+, Zn2+. J Environ Chem Eng. 2018;6(1):37–43.

56. Huang H, Li B, Li J, Zhang P, Yu W, Zhao N, et al. Influence of process parameters on the heavy metal (Zn2+, Cu2+ and Cr3+) content of struvite obtained from synthetic swine wastewater. Environ Pollut. 2019 Feb;245:658–65.

57. Angelici C, Meirer F, van der Eerden AMJ, Schaink HL, Goryachev A, Hofmann JP, et al. Ex Situ and Operando Studies on the Role of Copper in Cu-Promoted SiO2–MgO Catalysts for the Lebedev Ethanol-to-Butadiene Process. ACS Catal. 2015 Oct;5(10):6005–15.

58. Wang HC, Wei YL, Yang YW, Lee JF. XAS study of Zn-doped Al2O3 after thermal treatment. In: Journal of Electron Spectroscopy and Related Phenomena. Elsevier; 2005. p. 817–9.

59. Taifan WE, Li Y, Baltrus JP, Zhang L, Frenkel AI, Baltrusaitis J. Operando Structure Determination of Cu and Zn on Supported MgO/SiO 2 Catalysts during Ethanol Conversion to 1,3-Butadiene. ACS Catal [Internet]. 2019 Jan 4;9(1):269–85. Available from: https://doi.org/10.1021/acscatal.8b03515

60. Whitaker A. The crystal structure of hopeite, Zn 3 (PO 4) 2 .4H 2 O . Acta Crystallogr Sect B Struct Crystallogr Cryst Chem. 1975 Aug;31(8):2026–35.

61. Sato N, Minami T. State analysis related to zinc and manganese components in hopeite crystals of zinc phosphate films by XANES and EXAFS. J Mater Sci. 1989 Dec;24(12):4419–22.

62. Castorina E, Ingall ED, Morton PL, Tavakoli DA, Lai B. Zinc K-edge XANES spectroscopy of mineral and organic standards. J Synchrotron Radiat. 2019 Jul;26(4):1302–9.

63. Du W, Tan W, Yin Y, Ji R, Peralta-Videa JR, Guo H, et al. Differential effects of copper

nanoparticles/microparticles in agronomic and physiological parameters of oregano (Origanum vulgare). Sci Total Environ. 2018 Mar;618:306–12.

64. Arslanoglu H. Adsorption of micronutrient metal ion onto struvite to prepare slow release multielement fertilizer: Copper(II) doped-struvite. Chemosphere. 2019 Feb;217:393–401.

65. Pickup DM, Ahmed I, FitzGerald V, Moss RM, Wetherall KM, Knowles JC, et al. X-ray absorption spectroscopy and high-energy XRD study of the local environment of copper in antibacterial copper-releasing degradable phosphate glasses. J Non Cryst Solids. 2006 Aug;352(28–29):3080–7.

66. Hargreaves PR, Brookes PC, Ross GJS, Poulton PR. Evaluating soil microbial biomass carbon as an indicator of long-term environmental change. Soil Biol Biochem. 2003 Mar;35(3):401–7.

67. Xu Y, Tang H, Xiao X, Li W, Li C, Sun G, et al. Effects of long-term fertilization management practices on soil microbial carbon and microbial biomass in paddy soil at various stages of rice growth. Rev Bras Cienc do Solo. 2018;42.

68. Effects of heavy metals on soil microbial community - IOPscience.

69. Xie Y, Fan J, Zhu W, Amombo E, Lou Y, Chen L, et al. Effect of Heavy Metals Pollution on Soil Microbial Diversity and Bermudagrass Genetic Variation. Front Plant Sci. 2016 May;7(MAY2016):755.

70. Wang YP, Shi JY, Wang H, Lin Q, Chen XC, Chen YX. The influence of soil heavy metals pollution on soil microbial biomass, enzyme activity, and community composition near a copper smelter. Ecotoxicol Environ Saf. 2007 May;67(1):75–81.

71. Wolinska A, Stepniewsk Z. Dehydrogenase Activity in the Soil Environment. Dehydrogenases. 2012;

72. Łukowski A, Dec D. Influence of Zn, Cd, and Cu fractions on enzymatic activity of arable soils. Environ Monit Assess. 2018 May;190(5):278.

73. Chaperon S, Sauvé S. Toxicity interaction of metals (Ag, Cu, Hg, Zn) to urease and dehydrogenase activities in soils. Soil Biol Biochem. 2007 Sep;39(9):2329–38.

74. Szymá Nska M, Szara E, As AW˛, Sosulski T, Van Pruissen GWP, Cornelissen RL. Struvite-An Innovative Fertilizer from Anaerobic Digestate Produced in a Bio-Refinery.

75. Quilchano C, Marañón T. Dehydrogenase activity in Mediterranean forest soils. Biol Fertil Soils. 2002 Apr;35(2):102–7.

76. Bachmann S, Gropp M, Eichler-Löbermann B. Phosphorus availability and soil microbial activity in a 3 year field experiment amended with digested dairy slurry. Biomass and Bioenergy. 2014 Nov;70:429–39.

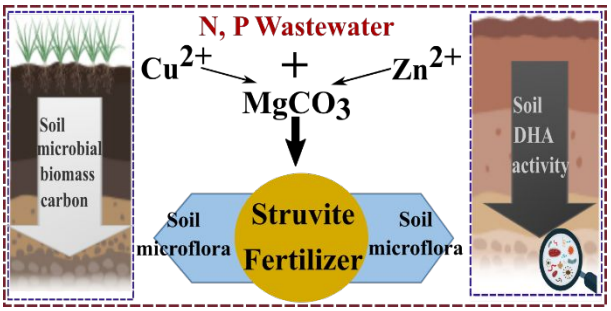

Magnesite has been used to produce struvite from nutrient rich wastewater in the presence of Cu^{2+} and Zn^{2+}, and the effects of this fertilizer material on soil microflora has been reported.